Biomaterials 257 (2020) 120233

Contents lists available at ScienceDirect

Biomaterials

journal homepage: www.elsevier.com/locate/biomaterials

# Hydrogel-mediated co-transplantation of retinal pigmented epithelium and photoreceptors restores vision in an animal model of advanced retinal degeneration

Nikolaos Mitrousis [a,b], Sabiha Hacibekiroglu [c,d], Margaret T. Ho [a,b], Yves Sauvé [e], Andras Nagy [c,d,f], Derek van der Kooy [b,d,g], Molly S. Shoichet [a,b,d,h,i,*]

[a] Institute of Biomedical Engineering, University of Toronto, Toronto, ON, M5S 3G9, Canada
[b] Donnelly Centre for Cellular and Biomolecular Research, University of Toronto, Toronto, ON, M5S 3E1, Canada
[c] Lunenfeld-Tanenbaum Research Institute, Mt Sinai Hospital, Toronto, ON, M5G 1X5, Canada
[d] Institute of Medical Science, University of Toronto, Toronto, ON, M5S 1A8, Canada
[e] Department of Ophthalmology and Visual Sciences, University of Alberta, Edmonton, AB, T6G 2R7, Canada
[f] Department of Obstetrics and Gynaecology, University of Toronto, Toronto, ON, M5G 1E2, Canada
[g] Department of Molecular Genetics, University of Toronto, Toronto, ON, M5S 1A8, Canada
[h] Chemical Engineering and Applied Chemistry, University of Toronto, Toronto, ON, M5S 3E5, Canada
[i] Department of Chemistry, University of Toronto, Toronto, ON, M5S 3H6, Canada

ARTICLE INFO

*Keywords:*
Hydrogel
Retinal regeneration
RPE
Co-transplantation
Photoreceptors
Blindness

ABSTRACT

We demonstrate a novel approach to reverse advanced stages of blindness using hydrogel-mediated delivery of retinal pigmented epithelium (RPE) and photoreceptors directly to the degenerated retina of blind mice. With sodium iodate ($NaIO_3$) injections in mice, both RPE and photoreceptors degenerate, resulting in complete blindness and recapitulating the advanced retinal degeneration that is often observed in humans. We observed vision restoration only with co-transplantation of RPE and photoreceptors in a hyaluronic acid-based hydrogel, and not with transplantation of each cell type alone as determined with optokinetic head tracking and light avoidance assays. Both RPE and photoreceptors survived significantly better when co-transplanted than in their respective single cell type controls. While others have pursued transplantation of one of either RPE or photoreceptors, we demonstrate the importance of transplanting both cell types with a minimally-invasive hydrogel for vision repair in a degenerative disease model of the retina.

## 1. Introduction

The RPE and photoreceptors of the retina have a well-established symbiotic relationship [1]. Classic studies [2,3] and observations of disease pathology demonstrate that their development and function are coordinated, and that deficits in either cell type lead to degeneration of both and the onset of blindness. Age-related macular degeneration (AMD) is believed to originate in dysfunction of the RPE [4], which eventually compromises the photoreceptors and leads to blindness. Conversely, retinitis pigmentosa is primarily caused by mutations in rod photoreceptors, causing cell death and leading to alterations in the RPE [5]. Advanced stages of blindness are characterized by impairment of both RPE and photoreceptors.

The retina comprises a well-organized laminar structure of seven distinct cell types, which largely remain intact [6], even after RPE and photoreceptor degeneration in diseased retinas. This has generated the impetus for cell transplantation to replace the exact cells lost at the correct retinal layer with the goal of re-establishing vision [7,8]. To date, the focus has been on transplanting either cell type alone, employing animal models that exhibit dysfunctions only in the respective cell type [9] or performing transplants at early time points along the course of degeneration, before the onset of blindness [10]. Some of these models have suffered from material transfer, which has confounded the interpretation of previous results [11–13]. Notably, photoreceptor transplantation has successfully been performed in models exhibiting complete degeneration of host photoreceptors [9,14–16]. However, these models do not recapitulate advanced stages of human retinal degeneration such as AMD, since the RPE remains unaffected.

* Corresponding author.Institute of Biomedical Engineering, University of Toronto, Toronto, ON, M5S 3G9, Canada.
*E-mail address:* molly.shoichet@utoronto.ca (M.S. Shoichet).

https://doi.org/10.1016/j.biomaterials.2020.120233
Received 8 April 2020; Received in revised form 7 July 2020; Accepted 10 July 2020
Available online 30 July 2020

Cells have been typically transplanted in the retina as either cell suspensions in solution [10,17,18] or cell grafts on sheets [19–22]. While transplanted grafts have led to better cell survival [21,23], the surgical strategy is complex, requiring custom-made delivery tools, and is more invasive than injection through a fine needle [21,24,25]. This increases the risk of damaging the already compromised retinal tissue. For example, increased immune responses have been observed at early time points after implantation of RPE grafts, compared to RPE suspensions [26]. Furthermore, clinical complications potentially associated with the graft transplantation surgery have been observed in patients [19,27]. An ideal delivery strategy would combine the improved survival afforded by graft transplantation with the minimal invasiveness of needle injection.

A shear-thinning, injectable hydrogel can protect the cells as they are deployed through the syringe needle into tissue [28,29]. Hyaluronan, a shear-thinning polymer, has been shown to promote the survival of photoreceptor cells both *in vitro*, through activating the mTOR pathway, and *in vivo*, through a CD44-mediated mechanism [30,31]. Despite these beneficial effects, HA does not form a gel on its own, which would lead to quick diffusion away from the injection site. Methylcellulose (MC), an inverse thermal gelling and biocompatible polymer, when mixed with HA, gives rise to a physical HAMC blend which gels after injection at physiological temperature [32]. HAMC enables local delivery of cells through a fine, 34-gauge syringe needle, with greater survival and tissue distribution than saline injection and without the complexity of graft transplantation [30].

Here, we injected RPE and photoreceptors, dispersed in a HAMC hydrogel, into the subretinal space of an advanced retinal degeneration mouse model. Sodium iodate ($NaIO_3$) treated mice exhibit advanced retinal degeneration of both RPE and photoreceptors, resulting in complete blindness [33,34]. We first validated the model by characterizing the temporal onset of blindness, and then used it to test the hypothesis that co-transplanting RPE and photoreceptors is superior to transplanting either cell type alone. We performed cell transplantation in animals exhibiting complete degeneration of the RPE, and severe, but not full, loss of photoreceptors in order to recapitulate, to the extent possible, the disease state frequently observed clinically in dry AMD patients [35]. We used RPE derived from hES cells, which have been shown to rescue vision in genetic (but not degenerative) models of RPE dysfunction [10] and have shown some benefit in clinical trials [17]. Despite recent advances in deriving photoreceptors from human pluripotent stem cell populations [15,36–39], more research is needed to identify a developmental stage for transplantation of these cells where survival and integration are optimal. We therefore used primary rod photoreceptors derived from the post-natal day 6 (P6) Nrl-GFP mouse retina, which have been successfully employed in transplantation studies [8,18,40].

## 2. Materials and methods

### 2.1. Animals

Experimental procedures were performed in accordance with the guide to the care and use of experimental animals and approved by the animal care committee at the University of Toronto.

Animals were randomized before the initiation of the studies to minimize within-cage effects, and all experiments were performed in a blinded fashion.

$NaIO_3$ (Sigma) was administered intravenously via the tail vein in 8–10 week old female C57Bl/6J mice (Charles River) as a 1% sterile-filtered (0.22 μm syringe filter, Millipore) solution in saline, at 70 mg/kg. Control mice were injected with saline.

To prevent weakness and dehydration of $NaIO_3$-treated animals treated with CsA, mice were kept on a 9% fat diet (Teklad 2019, Envigo) with daily mash (made with hydrated powder of Teklad 2019) provided for 2 weeks after $NaIO_3$ administration and during immune suppression. Animal weight was monitored frequently and animals that were below 20 g were not used for the cell transplantation studies. CsA was administered by osmotic minipumps (as opposed to bolus injections) to reduce CsA-associated morbidity. Osmotic minipumps (Alzet 2006 or 1004) were loaded with CsA (LC laboratories) in a solution of 65% ethanol, 35% Cremophor-EL (Sigma) and implanted in mice subcutaneously, 4 days before cell transplantation. Both the $NaIO_3$-treated and wild type animals were implanted with CsA pumps. The concentration of CsA loaded in the pumps was calculated using the Alzet Drug concentration calculator to deliver 10 mg/kg/day. The pumps were replaced according to the indicated release duration provided by Alzet (6 weeks for Alzet 2006 and 4 weeks for Alzet 1004). For pump implantation, the animals were brought to a surgical plane of anaesthesia with isoflurane. The pumps were implanted subcutaneously in the lower back area of the animals through a small mediolateral incision. Ketoprofen (5 mg/kg) was administered once daily for 2 days after the surgery. After pump implantation, and until the end of the study, animals were monitored daily for signs of distress or weakness. Animals that appeared dehydrated were provided with subcutaneous fluids (lactated Ringer's solution) 3 times daily (this was required for 3 animals).

Our subretinal transplantation success rate was 80%. Subretinal transplantations were considered unsuccessful when cell backflow into the vitreous or excessive bleeding was observed. Animals with unsuccessful transplantations were not included in the analysis. After cell transplantation, the animals received Ketoprofen (5 mg/kg) once daily for 2 days.

### 2.2. Rod photoreceptor sorting

The Nrl-GFP [41] transgenic mice were generously donated by Dr. Swaroop. Rod photoreceptors were isolated from P6 Nrl-GFP mice as described previously [31]. Briefly, eyes were dissected and the retinas were dissociated into a single-cell suspension by using a papain kit (Worthington). Fluorescent sorting was then performed for $GFP^+$/7-$AAD^-$ cells on a BD FACS Aria II sorter.

### 2.3. RPE differentiation

RPE were differentiated from H9 hES cells as described previously [42]. Briefly, the hES cells were grown in feeder-free conditions on Geltrex™ (ThermoFisher Scientific)-coated plates to confluence for 10–12 days in mTESR medium (Stem Cell Technologies), at which point the culture medium was switched to a differentiation medium containing 13% knock-out serum replacement (KSR), 1% Glutamax, 1% non-essential amino acids and 0.1% β-mercaptoethanol in Knock-out DMEM (all from ThermoFisher Scientific) in the absence of bFGF. The cell medium was replaced on alternate days. After approximately 1 month of culture, pigmented clusters started to appear in the wells. After an additional month of culture, these clusters became enlarged and more numerous. The pigmented clusters were manually isolated with a scalpel under a dissecting microscope, and plated in new Geltrex™-coated wells in medium containing 5% Hyclone FBS (ThermoFisher Scientific), 7% KSR, 1% Glutamax, 1% non-essential amino acids, 0.1% β-mercaptoethanol and 10 ng/ml bFGF (R&D Systems). For additional purity, these pigmented clusters were allowed to grow in culture for 1 additional month and the centers of the clusters, which exhibited the strongest RPE-like cobblestone morphology, were manually isolated for a second time. From this point onwards, the cells were considered to be RPE. For transplantation studies, only cells that had been passaged twice (P4) were used. The cells used for transplantation were kept at confluence for 1 month after their last passage in order for them to reacquire a cobblestone morphology.

ARPE19 were cultured in DMEM with 4.5 g/l glucose and glutamax, supplemented with 10% Hyclone FBS (all from ThermoFisher Scientific). The cell medium was replaced on alternate days, and cells were passaged using 0.05% trypsin (ThermoFisher Scientific). RNA was

isolated from cells after they had reached confluence.

### 2.4. HAMC cell delivery vehicle

A physical blend of hyaluronan (HA, 1200–1900 kDa; Novamatrix) and methylcellulose (MC, 300 kDa, Shin-Etsu) was used to prepare HAMC, as previously described [30]. Briefly, 24 h before use, sterile filtered HA and MC were dissolved into Hank's Balanced Salt Solution (HBSS) without calcium chloride, magnesium chloride and magnesium sulfate (ThermoFisher Scientific) at a concentration of 1% w/v, mixed in a SpeedMixer (DAC 150 FVZ; Siemens) for 30 s and left at 4 °C overnight. HAMC was mixed with cell solutions (in HBSS) to bring the final concentration to 0.5% w/v for each of HA and MC based on previous results demonstrating that this HAMC formulation improves cell survival and distribution after subretinal transplantation [30]. Prior to use, the HAMC-cell mixture was kept on ice for all experiments.

### 2.5. Cell transplantation

The experimental overview of the animal transplantation studies is shown in Scheme 1 (created with biorender.com). Subretinal transplantation was performed by a *trans*-vitreal approach. The cells were washed with HBSS and resuspended in HAMC at a final concentration of 12,500 cells/μl for RPE and 25,000 cells/μl for Nrl-GFP photoreceptors. Injections were performed into $NaIO_3$-treated animals that had been fitted with CsA minipumps. Animals were brought to a surgical plane of anaesthesia with isoflurane. Using a 34-gauge beveled needle attached to the Nanofilsubmicrolitre injection system (World Precision Instruments), 2 μL of cell suspension was injected into the sub-retinal space of the animals using a Möller Hi-R 900C surgical microscope (Innova Medical Ophthalmics). The injection was performed at a rate of 0.03 μl/s and the needle was kept in place for an additional minute after injection completion to limit backflow.

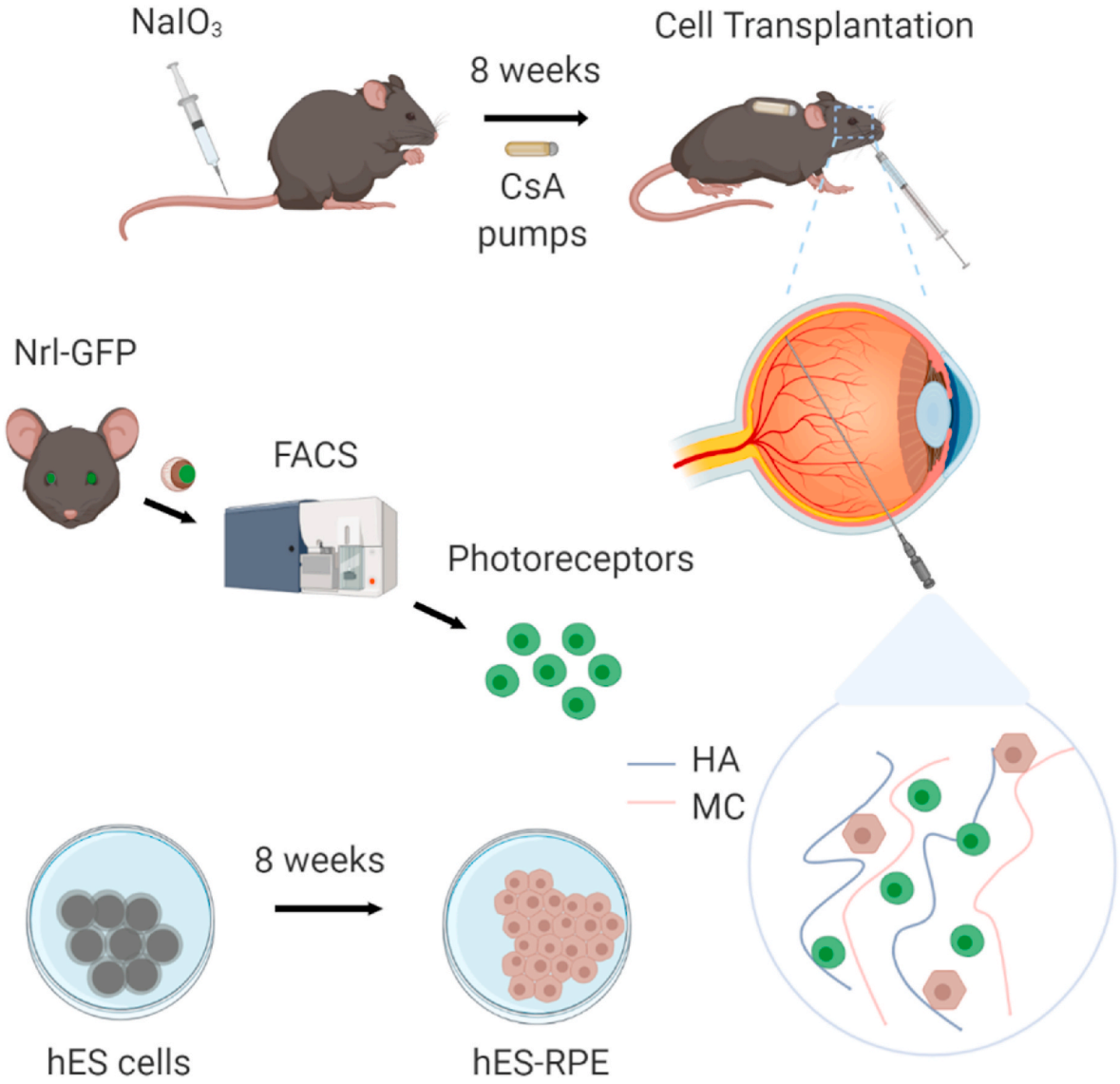


**Scheme 1.** Outline of the experimental procedures followed for the animal studies. Animals have sodium iodated injected in the tail vein and then have CsA, cyclosporin A, pumps inserted in order to immunosuppresses mice prior to cell transplantation. Primary rod photoreceptors are derived from Nrl-GFP mice while retinal pigmented epithelial (RPE) cells are differentiated from human embryonic stem (hES) cells and mixed with a physical blend of hyaluronan (HA) and methylcellulose (MC).

### 2.6. Optokinetic head tracking

Visual thresholds were measured by using the OptoMotry system (Cerebral Mechanics) [43]. Vertical sine gratings are projected on monitors as a virtual cylinder which surrounds an unrestrained mouse, placed on a platform. The rotation of the cylinder (12°/sec) elicited tracking behavior that was scored by a blinded observer watching through live video. For visual acuity measurements, the grating contrast was kept at 100%. Spatial frequency was measured for each eye separately using a staircase paradigm provided by the OptoMotry software, which varied the spatial frequency from 0.003 c/d to 0.642 c/d. The left eye tracks rotation in the clockwise direction while the right eye tracks rotation in the counter-clockwise direction. The experimenter was blinded to the direction of rotation and the spatial frequency of sine gratings being projected on the screens. The luminance level inside the OptoMotry apparatus was measured at ~200 lux, which falls well into the photopic range [44]. Unless otherwise stated, OKT was performed in photopic conditions. Scotopic illuminance levels can vary depending on the behavioral assay used. For scotopic conditions testing, the animals were dark adapted for 2–10 h and the experiments were performed in a completely dark room (no red lights). Neutral density filters (Lee filters) were used to decrease the luminance level inside the OptoMotry apparatus to <1.5 lux, which falls in the scotopic range for this assay [44]. To assess the scotopic tracking behavior, an infrared-sensitive camera was used (Sony Handycam DCR-HC28; Sony).

Each animal was tested until a reliable visual threshold could be established. In the complete absence of tracking, animals were tested for at least 7 min or 4 times in each direction of rotation, whichever was longest. Most sessions lasted between 10 and 20 min per animal. Each testing session consisted of multiple trials, during which the animal was presented with rotating sine gratings for up to 20 s or until tracking was observed. After each trial the sine gratings were turned off and the screens projected 50% gray for 4 s before the next trial began. For each weekly time point, each animal was tested at least 2 times on different days for each lighting condition. The OptoMotry chamber was thoroughly cleaned with Preempt cleaning solution (Virox Technologies) before and after each test.

### 2.7. Light avoidance assay

The light avoidance assay was performed on a custom-modified place conditioning apparatus (SOF-700RA-25 Two Chamber Place Preference Apparatus; Med Associates). One environment was black and the other was white, both with a metal rod floor. A removable partition containing a small aperture was positioned between the 2 environments such that the animals could move freely. The mice were placed in the middle compartment facing towards the wall of the chamber so as not to influence their preference. Mice were dark-adapted for 2–10 h and received a drop of 1% tropicamide (Mydriacyl, Alcon) on each eye 5–10 min before being placed in the chambers. The testing was performed in a completely dark room (no red lights). The animals were initially familiarized with the chambers by being placed in them for 10 min without any recording. On a different day, the animals were placed in the chambers for 10 min and their background preference for white or black compartment was recorded, in the absence of any stimulus. 4 weeks after cell transplantation, a single 10-min preference test session was performed and the time spent in each compartment, the average activity in each compartment, the number of transitions and the fecal boli produced by the mice were recorded. The white compartment was illuminated from above with a white LED lamp (Sylvania) that was covered with neutral density filters (Lee Filters) resulting in an illumination level of ~10 lux at the chamber floor. This illumination level has previously been used for scotopic testing in light avoidance assays [15]. No illumination could be detected in the black compartment. Both compartments were covered with custom-made light-impermeable lids, and the lid of the white (lit) compartment contained a transparent, circular area of 6 cm in diameter through which the light seeped into the chamber. For the background testing, the transparent circular area was covered so that the lids of both compartments were completely light-impermeable. No temperature differences were detected in the lit vs dark compartments after 8 h of testing. The chambers were thoroughly cleaned with 70% ethanol before and after each test.

The light avoidance index presented in the results was calculated as:

- [(% of time spent in lit white chamber) – (% of time spent in unlit white chamber by background preference)].

### 2.8. Electroretinography

The animals were dark-adapted overnight (12–15 h), and prepared for bilateral ERG recordings under dim red light. Anaesthesia was induced with a mixture of ketamine (150 mg/kg) and xylazine (10 mg/kg), injected intraperitoneally. The head was secured with a stereotaxic holder and the body temperature was maintained at 38 °C, using a homeothermic blanket. Pupils were dilated using 1% Tropicamide (Mydriacyl, Alcon). A drop of 0.9% saline was applied on each cornea to prevent dehydration and to allow electrical contact with the recording electrode (gold wire loop). A 25-gauge platinum needle inserted subdermally behind the eyes served as reference electrode. Simultaneous bilateral recording was achieved with active gold loop electrodes placed on each cornea. Amplification (at 1–1000 Hz bandpass, without notch filtering), stimulus presentation, and data acquisition were performed by the Espion $E^2$ system (Diagnosys). Stimuli consisted of single white (6500 K) flashes (10 μs duration), repeated 3–5 times to verify the responsiveness reliability. For scotopic responses, stimuli were presented at 19 increasing intensities varying from −5.2 to 2.9 log cd/$m^2$ in luminance. To allow for maximal rod recovery between consecutive flashes, inter-stimuli-intervals were increased (as the stimulus intensities were progressively increased) from 10 s at lowest stimulus intensity up to 2 min at highest stimulus intensity. After the scotopic recordings were completed, a 30 cd/$m^2$ background stimulus was applied and photopic responses were studied. Single flashes with intensities ranging from −1.6 to 2.9 log cd/$m^2$ along 11 steps of incremental intensities were presented.

### 2.9. Immunohistochemistry and quantification

Animals were sacrificed by an overdose of sodium pentobarbital, followed by transcardial perfusion with ice cold PBS and 4% paraformaldehyde (PFA), sequentially. The eyes were enucleated and kept in 4% PFA overnight at 4 °C. The following day, the eyes were thoroughly washed with PBS and placed in a 30% sucrose solution overnight at 4 °C. After being embedded in Tissue-Tek OCT compound (Sakura), the eyes were flash-frozen in dry ice-cooled 2-methyl-butane and serially sectioned to 14 μm using a Leica CM3050S cryostat. Every fifth section from each eye was used for staining and quantification. On average, 45 sections from each eye were analyzed. In some experiments, the eyes were dissected, neural retinas removed, and the eye cups containing the RPE were flatmounted. The antibodies used in this study are listed on Table 1 bellow. Rhodamine-conjugated phalloidin (ThermoFisher R415) was used at 1:100. Images for quantification were acquired using a Zeiss AxioScan.Z1 slide scanner. Quantification was conducted by using Fiji [45], following a previously validated method [46]. Regions of interest (ROIs) were drawn to encompass either the outermost layer of the retina (inner nuclear layer and occasional patches of remaining outer nuclear layer) for transplanted photoreceptor quantification or the subretinal space (between the outermost layer of the retina and the choroid) for RPE quantification. Transplanted cells found in other areas such as the vitreous or the choroid, were rare and not included in the analysis. The injection site was also excluded from the analysis. All ROIs were manually inspected and any staining that did not correspond to a $Hoechst^+$ cell was excluded. We first quantified the number of STEM121

**Table 1**
Antibodies used in this study.

| Target | Manufacturer | Cat No. | Dilution | Host | Reactivity |
|---|---|---|---|---|---|
| *STEM121* | Takara Bio | Y40410 | 1:2000 | Mouse | Human |
| *GFP* | Rockland | 600-101-215 | 1:500 | Goat | GFP, rGFP, eGFP |
| *PRPH2* | Proteintech | 18109-1-AP | 1:750 | Rabbit | Mouse, Human |
| *RPE65 (in vivo)* | Millipore | MAB5428 | 1:250 | Mouse | Mouse, Human |
| *RPE65 (in vitro)* | Novus Biologicals | NB100-355 | 1:200 | Mouse | Mouse, Human, |
| *PKCα* | Sigma-Aldrich | P4334 | 1:10,000 | Rabbit | Mouse |
| *Calbindin (D28K)* | Santa Cruz Biotechnology | Sc-7691 | 1:1000 | Goat | Mouse, Human |
| *Rhodopsin* | Millipore | MAB5316 | 1:250 | Mouse | Mouse, Human, |
| *Recoverin* | Millipore | AB5585 | 1:1000 | Rabbit | Mouse, Human |
| *Otx2* | R&D Systems | BAF1979 | 1:100 | Goat | Mouse, Human |
| *Bestrophin* | Novus Biologicals | NB300-164 | 1:200 | Mouse | Human |
| *ZO-1* | Life Technologies | 40–2200 | 1:100 | Rabbit | Mouse, Human |

or GFP-positive pixels in each eye, using Fiji algorithms ("moments" for STEM121 quantification and "Huang" for GFP quantification) that were chosen based on their effectiveness at discriminating between positive signal and background staining in control slides. We next calculated the average pixel size of a single $STEM121^+$ or $GFP^+$ cell, by drawing small ROIs only encompassing one cell and quantifying pixel size by the "moments" or "Huang" algorithm, respectively. To ensure accuracy, we quantified the size of ≥25 individual cells for each cell type, using images from all conditions and multiple animals. On average, the size of a $STEM121^+$ cell was 36.37 (±7.62) pixels, and the average size of a $GFP^+$ cell was 29.47 (±4.05) pixels. Last, we calculated the number of $STEM121^+$ or $GFP^+$ cells per eye by dividing the total number of $STEM121^+$ or $GFP^+$ pixels by the average size of a single cell, respectively. By following this approach, we could maximize the tissue area analyzed since we were using the entirety of the retinal area of ~45 sections for each calculation, as opposed to imaging randomly selected fields of each section, which may introduce bias. Images for demonstration were acquired on an Olympus Fluoview FV1000 confocal microscope.

ONL thickness was quantified within a ~1000 μm region from the optic nerve head. In each section the thickness was measured in 3 random areas within the 1000 μm region. At least 8 sections were used for each eye.

### 2.10. Quantitative real-time PCR

RNA was isolated using Trizol (Life Technologies), following the manufacturer's instructions. After RNA extraction, DNAse treatment was done with TurboDNAse (Ambion). The quality of the purified RNA was assessed by measuring the 260/280 ratio on a spectrophotometer (ND-1000, Nanodrop). Only RNA with a 260/280 ratio >1.8 was used. RNA was reverse transcribed using the superscript VILO cDNA synthesis kit (Life Technologies). qPCR amplification was done in an Applied Biosystems 7900HT instrument using SYBR Green Master Mix (Roche). Melting curves were performed for each experiment and negative controls (no RT enzyme controls and no template controls) were always included to ensure the accuracy of the results. The primer pairs used were as follows: *MITF FP* TTGTCCATCTGCCTCTGAGTAG, *MITF RP* CCTATGTATGACCAGGTTGCTTG, *OTX2 FP* ACCTTGAACTCCACC TCTGC, *OTX2 RP* GCTTCTCTTCTCTGACTCTCTTTG, *RPE65 FP* TACAGAAAGCACTGAGTTGAGC, *RPE65 RP* CCATTTAGTAAGTCCACATTC ATTTCC, *CRALBP FP* AGATCTCAGGAAGATGGTGGAC, *CRALBP RP* GAAGTGGATGGCTTTGAACC, *PEDF FP* TATCACCTTAACCAGCCTTTCATC, *PEDF RP* GGGTCCAGAATCTTGCCAATG, *PMEL17 FP* GTTG ATGGCTGTGGTCCTTG, *PMEL17 RP* CAGTGACTGCTGCTATGTGG, *TYR FP* GTGTAGCCTTCTTCCAACTCAG, *TYR RP* GTTCCTCATTACCAAATAGCATCC, *NANOG FP* CCCTCCTCCCATCCCTCATAG, *NANOG RP* TCGCTGATTAGGCTCCAACC, *OCT4 FP* CTGTCTCCGTCACCACTCTG, *OCT4 RP* TGTGTTCCCAATTCCTTCCTTAG, *GAPDH FP* AGCAAGAGCACAAGAGGAAGAG, *GAPDH RP* GAGCACAGGGTACTTTATTGATGG, *HMBS FP* TGCTATCTGGGGAGTGATTACC, *HMBS RP* GGCTGT TGCTTGGACTTCTC. Quantification was performed using the ΔΔCt method; GAPDH and HMBS were used as housekeeping genes. The relative expression shown is the average of the $2^{-\Delta\Delta Ct}$ values calculated for each housekeeping gene.

### 2.11. Statistical analysis

All data are reported as mean ± standard error of the mean unless otherwise indicated. Statistical analysis was performed using GraphPad Prism software. N represents number of animals, n represents number of eyes, where appropriate. For comparisons between multiple groups, an analysis of variance (ANOVA) followed by Tukey's (for 1-way ANOVA) or Bonferroni (for 2-way ANOVA) post-hoc test was used. For comparisons between two groups, a Student's t-test was used. For comparison between groups with unequal variances, a non-parametric Mann Whitney test was used to compare two groups. Three statistically significant outliers by Grubb's test (1 eye in HAMC and 1 eye in the Uninjected group for the OKT data, 1 eye in the Photo + RPE group for the RPE quantification data) were excluded from the analysis. A p-value of $<0.05$ was regarded as statistically significant ($^*p < 0.05$, $^{**}p < 0.01$, $^{***}p < 0.001$).

## 3. Results

### 3.1. Sodium iodate induces retinal degeneration

We injected $NaIO_3$ intravenously and assessed mouse visual function over time by optokinetic head tracking (OKT) and light avoidance assays (Fig. 1A). OKT is based on an innate reflex, whereby mice track the movement of rotating stripes by moving their head in the direction of the stripes [43]. OKT revealed a biphasic loss of visual acuity after $NaIO_3$ administration, with complete blindness evident by day 35 post-injection (Fig. 1B). The light avoidance assay is based on the natural aversion that mice exhibit towards lit spaces [47]. Mice were placed in a 2-compartment chamber with a connecting aperture where one compartment was lit and the other was dark. The decrease in time spent in the lit compartment upon provision of the light stimulus is a measure of light sensation, and was plotted as a "light avoidance index". This assay, performed on day 36 after $NaIO_3$ administration, corroborated the OKT results: $NaIO_3$-treated animals, relative to saline-treated mice, exhibited significantly decreased aversion to light (4.9-fold, $p < 0.01$), demonstrating diminished visual function (Fig. 1C).

We next analyzed the tissue histology of the $NaIO_3$-treated animals, 64 days after treatment, just before cell transplantation. We found complete degeneration of RPE cells as assessed by immunostaining for the RPE markers RPE65 and Otx2 on cryosections (Fig. 1D), flatmount preparations (Fig. 1E and Supplementary Fig. 1A), and H&E staining on cryosections (Supplementary Fig. 1B). We also observed a significant thinning of the outer nuclear layer (ONL) in treated animals (Fig. 1F): from 57 ± 1 μm in saline-treated controls to 16 ± 1 μm in $NaIO_3$-treated animals ($p < 0.001$, Fig. 1G); and from 11.0 ± 0.1 cell layers in saline-treated controls to 3.5 ± 0.1 cell layers in $NaIO_3$-treated animals ($p < 0.001$, Fig. 1H), indicating widespread photoreceptor death. Importantly, the rest of the retinal structure exhibited no apparent morphological differences from the controls based on immunohistochemistry (Fig. 1F and Supplementary Fig. 2). These data demonstrate that the $NaIO_3$ mouse model exhibits a phenotype that resembles advanced

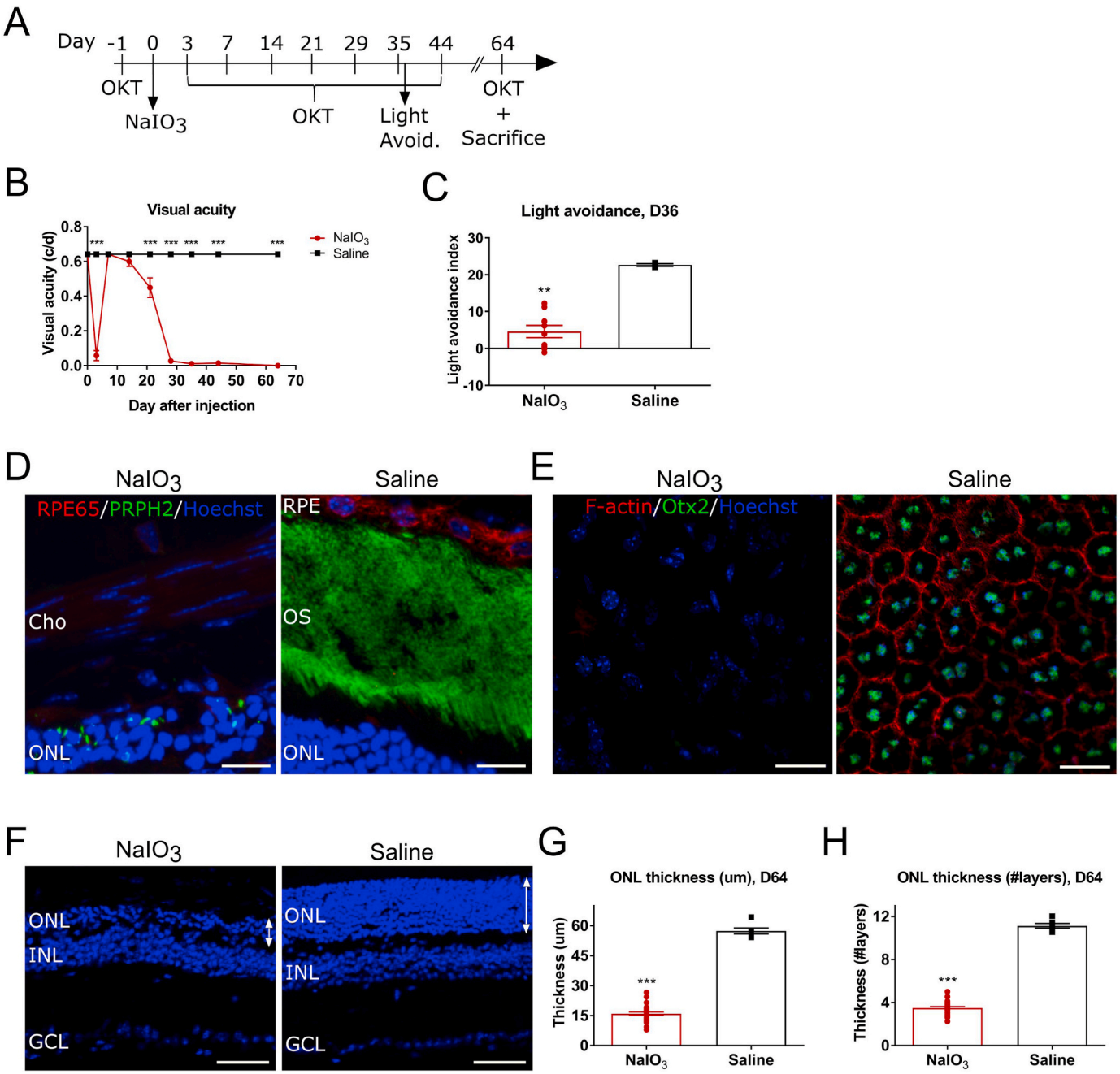


**Fig. 1.** $NaIO_3$ induces retinal degeneration at the behavioral and tissue levels. (A) Experimental timeline. OKT, optokinetic head tracking assay; Light Avoid, light avoidance assay. (B) Visual acuity measured by OKT over time shows complete loss of visual acuity after 35 days with $NaIO_3$ injection and no change with saline injection (mean ± SEM, n = 16 eyes for $NaIO_3$, n = 6 eyes for saline). Statistical significance was evaluated by 2-way ANOVA, with a Bonferroni post-hoc. ***$p < 0.001$. (C) Light avoidance assay demonstrates significantly decreased aversion to light after $NaIO_3$ administration vs. saline at day 36 (mean ± SEM, N = 9 animals for $NaIO_3$, N = 3 animals for saline). Statistical significance was evaluated by a 2-tailed, Mann Whitney test. **$p < 0.01$. The light avoidance index shown is the decrease in time spent in the lit compartment after provision of the light stimulus (see materials and methods). (D) Representative immunohistochemistry images of the subretinal space, RPE and choroid 64 days after $NaIO_3$ or saline injection, stained for the RPE marker RPE65 and the outer segment marker peripherin. ONL, outer nuclear layer; OS, outer segments; Cho, choroid. Scale bar is 15 μm. (E) Representative immunohistochemistry images of RPE flatmounts 64 days after $NaIO_3$ or saline injection, stained for the RPE marker Otx2 and the cytoskeletal marker F-actin, show the lack of RPE after $NaIO_3$ treatment. Scale bar is 25 μm. See also Supplementary Fig. 1A for wide-field images of the flatmount preparations. (F) Representative immunohistochemistry images of the retinal layers 64 days after $NaIO_3$ or saline injection. The arrows demonstrate the boundaries of the ONL that were used for quantification. ONL, outer nuclear layer; INL, inner nuclear layer; GCL, ganglion cell layer. Scale bar is 50 μm. (G) ONL thickness in μm or (H) in cell layers, 64 days after $NaIO_3$ or saline injection (mean ± SEM, n = 26 eyes for $NaIO_3$, n = 6 eyes for saline). Statistical significance was evaluated by a 2-tailed, unpaired *t*-test. ***$p < 0.001$.

retinal degeneration in the human at both behavioral and tissue levels.

### 3.2. *RPE differentiation from hES cells*

We derived RPE from hES cells because they can provide an unlimited and clinically relevant source of RPE. We followed the overgrowth

protocol [48] with minor modifications (Fig. 2A). The differentiated RPE (hES-RPE) established cobblestone monolayers that were pigmented, expressed the tight junction marker ZO-1 and the RPE-specific markers RPE65 and Bestrophin-1 (Fig. 2B).

Real-time quantitative PCR revealed a progressive upregulation of the RPE markers MITF, OTX2 and RPE65 at the RNA level over the course of differentiation (Fig. 2C). A comparison to the ARPE19 cell line, which is often used as a human RPE substitute [49], demonstrated that the hES-RPE expressed 25-fold more MITF ($p < 0.01$, Fig. 2C), 10-fold more OTX2 ($p < 0.001$, Fig. 2C) and 270-fold more RPE65 ($p < 0.001$, Fig. 2C). To investigate these differences further, we assessed the expression of the RPE markers CRALBP and PEDF, the RPE-melanocyte markers PMEL17 and TYR, and the pluripotency markers NANOG and OCT4 in hES, hES-RPE and ARPE19 cells (Fig. 2D). All four RPE markers were significantly upregulated in the hES-RPE compared to both hES cells (50–660-fold, $p < 0.01$) and ARPE19 cells (190–1620-fold, $p < 0.01$) (Fig. 2D). In contrast, the pluripotency markers were significantly downregulated (310–580-fold, $p < 0.001$) in hES-RPE compared to the originating hES cells, to levels similar to those found in ARPE19 cells (relative expression of NANOG: $1 \pm 0.1$ for hES-RPE vs $0.7 \pm 0.1$ for ARPE19; relative expression of OCT4: $1.2 \pm 0.2$ for hES-RPE vs $1.5 \pm 0.6$ for ARPE19) (Fig. 2D). Together, these data show that RPE were readily derived from hES cells and that they express higher levels of RPE markers than the ARPE19 cell line. It is possible that higher expression of RPE genes would be observed in ARPE19 cells if they had been kept in confluence for a significantly extended period [50].

### 3.3. Photoreceptor isolation from Nrl-GFP mice

We used P6 Nrl-GFP rods as our source of photoreceptors because these cells have been extensively studied for transplantation in the past [8,18] and there is no readily available source of transplantable human pluripotent stem cell-derived photoreceptors. Nrl is the fate-determining transcription factor of rod photoreceptors [41], hence GFP is specifically targeted to newborn rods in these mice (Fig. 2E). A flow cytometry purity check after fluorescence-activated cell sorting (FACS) for GFP revealed that our photoreceptor population was 97.2% $GFP^+$ (Fig. 2F).

### 3.4. RPE and photoreceptor co-transplantation induces visual recovery at the behavioral level

We performed transplantation experiments at 8 weeks after $NaIO_3$ treatment (Fig. 3A) - a time when mice were completely blind, as assessed by OKT (Fig. 3B), and the RPE and photoreceptors were degenerated. We transplanted 50,000 photoreceptors and/or 25,000 RPE per eye in a total volume of 2 μl of HAMC into the subretinal space. These numbers were chosen based on: i) previous experiments with single cell type transplants [10,30,40]; ii) pilot studies where we determined that a photoreceptor to RPE ratio of 2:1 is superior to higher ratios in terms of visual recovery (Supplementary Fig. 3); and iii) cell concentration limitations associated with injectability. A HAMC-injected group and a non-transplanted group ("Uninjected") served as vehicle and negative controls, respectively.

We assessed behavioral recovery after transplantation by OKT and light avoidance assays. Rod photoreceptors mediate scotopic visual responses while cones are responsible for photopic vision. To distinguish between the two, we performed OKT at both scotopic (<1.5 lux) and photopic (~200 lux) conditions. Interestingly, only the co-transplant group exhibited significant visual recovery 4 weeks after transplantation in scotopic conditions ($p < 0.001$, co-transplant vs uninjected; co-transplant vs HAMC; co-transplant vs photoreceptors alone) (Fig. 3B). While there was no significant difference between the co-transplanted RPE and photoreceptor in HAMC group vs. RPE alone in HAMC under scotopic conditions, there was also no significant difference observed between RPE alone and all of the other groups (i.e., photoreceptors alone, HAMC alone, uninjected), demonstrating the importance of replacing RPE and photoreceptors for some visual function restoration. No significant differences ($p > 0.05$) were identified between the groups at any time point after transplantation in photopic conditions (Fig. 3C), which was expected given that rods are responsible for night vision [44].

To corroborate our OKT data, we performed light avoidance testing in scotopic conditions (~10 lux) 4 weeks after transplantation. We analyzed the average mouse activity in the lit vs dark chambers. Mice are nocturnal and thus normally more active in the dark [51]. The only groups that were significantly more active in the dark chamber than the lit chamber were the co-transplant group and the wild type animals ($p < 0.05$, Fig. 3D). Like the wildtype animals, the co-transplant group avoided the lit compartment significantly more than the photoreceptor alone group (Fig. 3E). We observed a trend towards the photoreceptor alone group avoiding the lit chamber less than the uninjected group, but this did not reach statistical significance ($p = 0.57$). Importantly, no differences were observed between the groups in the number of entrances into the lit chamber ($p > 0.05$, Fig. 3F) or the number of fecal boli produced ($p > 0.05$, Fig. 3G). These data indicate that the differences observed in mouse activity were not mediated by anxiety [52], but rather demonstrate increased visual perception in the co-transplanted animals, which is similar to that of wildtype. Together, these data demonstrate, for the first time, that RPE and photoreceptor co-transplantation restores some functional scotopic vision in previously blind mice at an advanced stage of degeneration.

### 3.5. Co-transplantation leads to superior survival for both RPE and photoreceptors

To probe the mechanism underlying the observed behavioral effects, we assessed transplanted cell survival 2 months after transplantation by immunostaining for human-specific STEM121 to detect the hES-RPE and GFP to detect the donor photoreceptors. At this time point, the majority of the ONL was absent in most animals, with the exception of occasional patches of host photoreceptors, the number of which was not different among the groups and did not correlate with visual recovery (Supplementary Fig. 4). These host photoreceptors expressed the visual cycle markers rhodopsin and recoverin (Supplementary Fig. 5).

Both donor RPE and photoreceptors were more abundant when transplanted together than each alone; however, the overall percent survival was still low for both. Donor RPE formed pigmented monolayer-like structures that juxtapose the outermost layer of the host retina (Fig. 4A and Supplementary Fig. 6). Interestingly, co-transplantation led to a 2.8-fold increase in surviving RPE numbers of $2100 \pm 400$ vs $750 \pm 160$ for transplantation of RPE alone (**$p < 0.01$, Fig. 4B). Donor photoreceptors were found on the outer edge of the remaining inner nuclear layer (Fig. 4A). Notwithstanding their low abundance overall, co-transplantation resulted in a 2.1-fold increase in photoreceptor survival of $210 \pm 20$ vs $100 \pm 30$ for transplantation of photoreceptors alone (**$p < 0.01$, Fig. 4C). These photoreceptors expressed synaptophysin (Supplementary Fig. 7A) but not peripherin (Supplementary Fig. 7B) and did not exhibit a mature morphology. It is important to note that no double positive cells for GFP and STEM121 were identified, suggesting that material transfer did not occur between donor RPE and photoreceptors.

We wondered whether the increased cell survival of RPE and photoreceptors after co-transplantation would correlate with the maximum b-wave value obtained by scotopic electroretinography (ERG) in individual eyes and thus first characterized the electrical responses of the retina to light. Photoreceptor transplants can lead to light-driven *trans*-synaptic activation of depolarizing (ON) bipolar cells as reflected by recordable b-waves [53]. In wild type animals, the amplitude of b-waves grew proportionally to flash stimulus strength, saturating at 1.89 log $cd/m^2$ (Supplementary Figs. 8A and B). The co-transplant group showed an initial increase in b-wave amplitudes starting at $-2.82$ log $cd/m^2$, followed by saturation at 0.37 log $cd/m^2$ and gradual extinction at

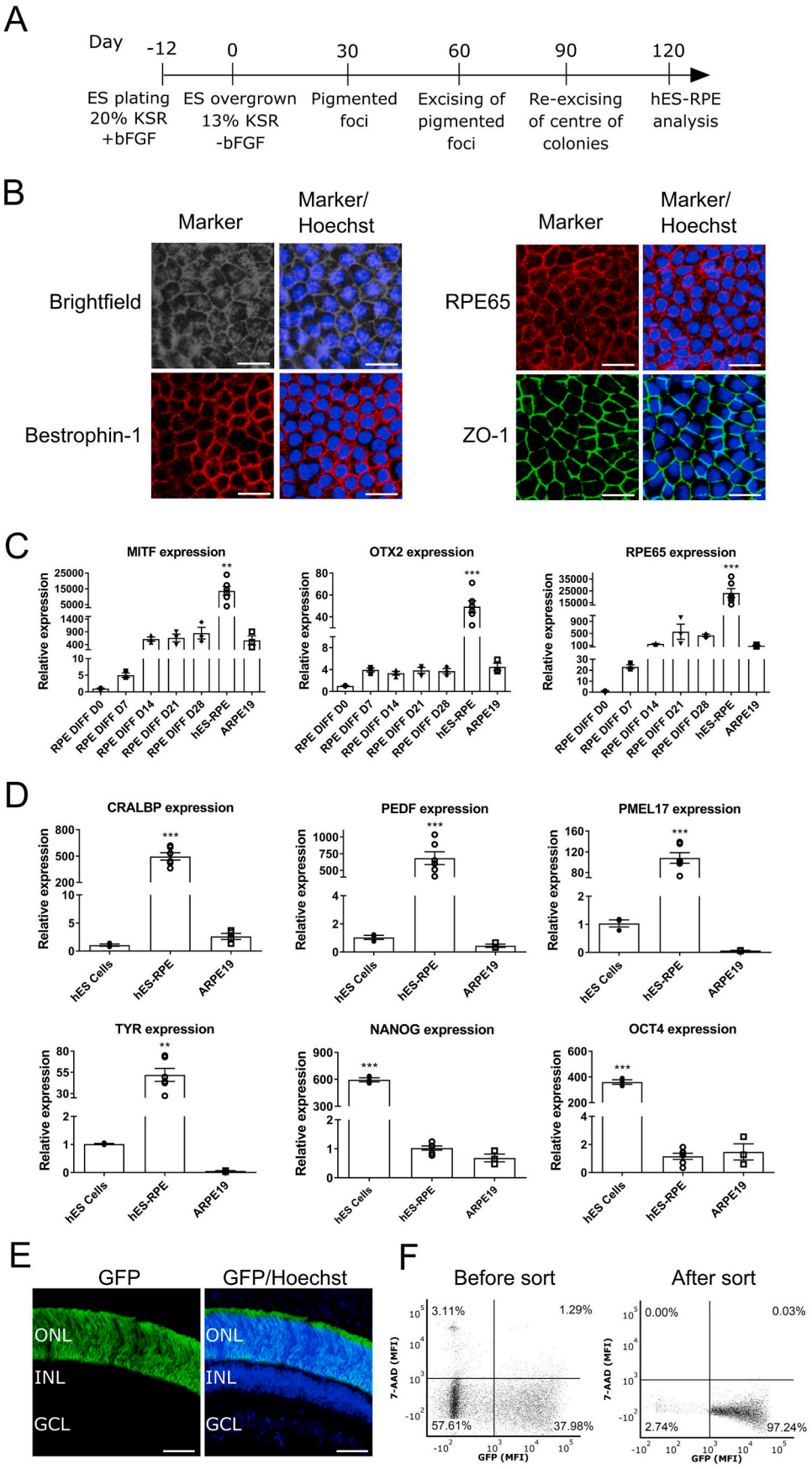


**Fig. 2.** RPE derivation from hES cells and photoreceptor isolation from Nrl-GFP mice. (A) Timeline of RPE differentiation from hES cells. KSR, knock-out serum replacement; bFGF, basic fibroblast growth factor. (B) Representative immunostaining pictures of hES-RPE, stained for the RPE markers Bestrophin-1, RPE65 and the tight junction marker ZO-1. Scale bar is 20 μm. (C) qPCR for the expression of the RPE markers MITF, OTX2 and RPE65 over the course of the differentiation protocol and in the ARPE19 cell line (mean ± SEM, n = 3–6 independent experiments). Statistical significance was evaluated by 1-way ANOVA with a Tukey's post-hoc. $^{**}p < 0.01$; $^{***}p < 0.001$. (D) qPCR for the expression of the RPE markers CRALBP, PEDF, the melanocyte markers PMEL17, TYR and the pluripotency markers NANOG, OCT4 in hES cells, hES-RPE and ARPE19 cells (mean ± SEM, n = 3–6 independent experiments). Statistical significance was evaluated by 1-way ANOVA with a Tukey's post-hoc. $^{**}p < 0.01$; $^{***}p < 0.001$. (E) Representative immunohistochemistry image of the retinal layers in an Nrl-GFP mouse, demonstrating GFP expression only in the ONL. ONL, outer nuclear layer; INL, inner nuclear layer; GCL, ganglion cell layer. Scale bar is 40 μm. (F) FACS plots demonstrating expression of GFP and the dead cell stain 7-AAD in P6 Nrl-GFP retinal preparations before and after FACS. MFI, mean fluorescence intensity.

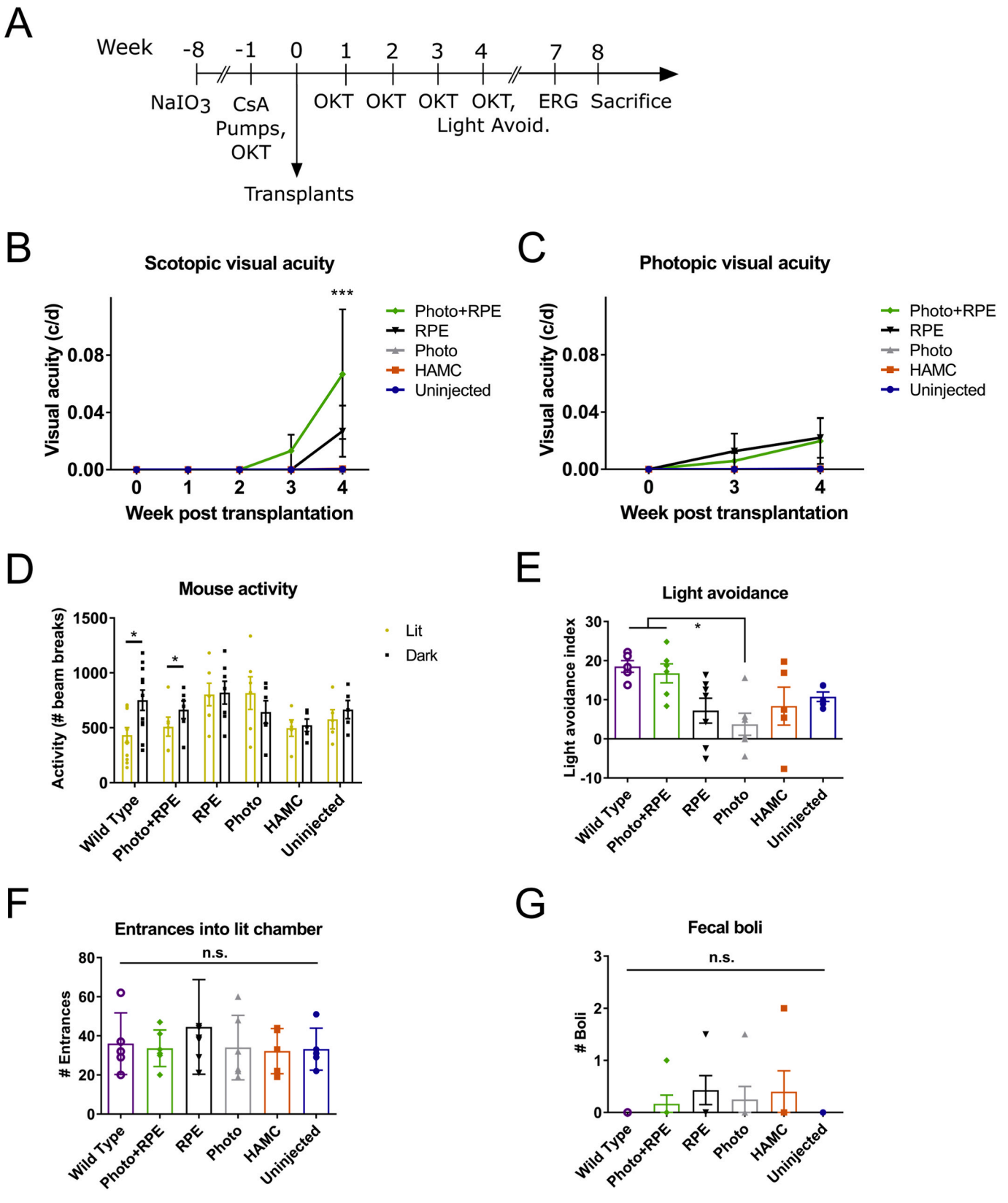


*(caption on next page)*

**Fig. 3.** RPE and photoreceptor co-transplantation leads to visual recovery. (A) Experimental timeline. CsA, cyclosporin A; OKT, optokinetic head tracking assay; Light Avoid. light avoidance assay; ERG, electroretinography. (B) Visual acuity in scotopic conditions over time after transplantation, assessed by OKT (mean ± SEM, n = 9–12 eyes). Statistical significance was evaluated by 2-way ANOVA with a Bonferroni post-hoc. ***p < 0.001 for Photo + RPE vs Uninjected, Photo + RPE vs HAMC, and Photo + RPE vs Photo. (C) Visual acuity in photopic conditions over time after transplantation, assessed by OKT (mean ± SEM, n = 9–12 eyes). As expected, a 2-way ANOVA with a Bonferroni post-hoc identified no significant effects. (D) Average mouse activity in the dark and lit chambers during the light avoidance assay, one month after transplantation (mean ± SEM, N = 5–7 animals), show that only wildtype and RPE + photoreceptor co-transplanted mice have visual function. Statistical comparisons between dark and lit chamber activity within each group were performed by 2-tailed, paired *t*-test. *p < 0.05. (E) Light avoidance index, one month after transplantation (mean ± SEM, N = 5–7 animals). Statistical significance was evaluated by one-way ANOVA with a Tukey's post-hoc. *p < 0.05 for Wild Type vs Photo, Photo + RPE vs Photo. (F) Average number of entrances into the lit chamber during the light avoidance assay, one month after transplantation (mean ± SEM, N = 5–7 animals). A one-way ANOVA with a Tukey's post-hoc identified no significant effects. (G) Average number of fecal boli produced during the light avoidance assay, one month after transplantation (mean ± SEM, N = 5–7 animals). A one-way ANOVA with a Tukey's post-hoc identified no significant effects.

higher light intensities (Supplementary Figs. 8C and D). This pattern is consistent with the occurrence of functional, albeit weak, phototransduction that gets saturated at higher flash strengths [54]. B-waves did not exceed the 40 μV criterion amplitude in any other groups (Supplementary Fig. 8E–L); and b-waves were not detected in the uninjected $NaIO_3$-treated animals (Supplementary Fig. 8K and L). We observed a positive correlation between the number of donor RPE and the ERG b-wave value ($p = 0.056$, Spearman $r = 0.37$, Fig. 5A), as well as a significant positive correlation between the donor photoreceptor number and ERG b-wave value ($p < 0.05$, Spearman $r = 0.43$, Fig. 5B). To assess whether the transplanted RPE affected the host photoreceptors, we performed correlation analyses between the donor RPE number and the area of peripherin$^+$ staining, which originates in the host photoreceptors (Supplementary Figs. 3 and 6B). Interestingly, we observed a positive correlation between donor RPE number and peripherin$^+$ area in the co-transplant group ($p = 0.099$, Pearson $r = 0.62$, Fig. 5C), and not in the RPE alone group ($p = 0.91$, Pearson $r = -0.04$, Fig. 5D).

## 4. Discussion

Advanced stages of retinal degeneration are characterized by pathological changes in RPE and photoreceptors. It has been previously demonstrated that either RPE or photoreceptor transplantation alone holds some promise for restoring vision in models of early retinal degeneration that exhibit defects in RPE or photoreceptors, respectively [10,18]; however, these genetic models do not reflect the pathology observed in human disease where degeneration of RPE and photoreceptors leads to blindness. We demonstrate the novel approach of transplanting RPE together with photoreceptors in an injectable biomaterial using a mouse model where both RPE and photoreceptors die. For the first time, to the best of our knowledge, we achieve some visual recovery in an animal model of complete blindness by dissociated cell co-transplantation. Unlike approaches where retinal sheets are transplanted [21,55], our hyaluronan-based hydrogel does not require the use of custom-made surgical tools and allows cell injection through a very fine, 34-gauge needle, minimizing the invasiveness of the surgery. Furthermore, dissociated cell transplantation allays concerns related to graft orientation or rosette formation, which has been extensively observed in retinal sheet transplants and may limit integration into the host tissue [36,56].

The lack of genetic animal models that faithfully reproduce advanced retinal disease, where both RPE and photoreceptors degenerate, has hindered studies into clinically relevant approaches to reverse it. We employed the $NaIO_3$ mouse model, in which the mechanism of RPE cell death after treatment has been studied [57]; yet, the temporal onset of blindness at the behavioral level after $NaIO_3$ injection has only been investigated in a few studies [34,58,59]. We found that the loss of vision after $NaIO_3$ treatment followed a biphasic profile where there was an acute decrease in visual acuity after injection, which recovered to baseline levels before the onset of a second, slower phase of decreasing visual acuity, ultimately resulting in blindness after 35 days. This pattern has been observed before [58–60], but its underlying cause remains elusive; we hypothesize that necrotic RPE death, which occurs soon after $NaIO_3$ administration [61], leads to accumulation of debris in the subretinal space, which impairs vision. Clearance of the debris allows vision to resume temporarily, until the loss of RPE triggers photoreceptor death, resulting in functional blindness. The cell death kinetics of RPE and photoreceptors after $NaIO_3$ injection was reflected at the behavioral level. At the time of cell transplantation, 2 months after $NaIO_3$ treatment, virtually all host RPE and most host photoreceptors were absent, eliminating the possibility for material exchange observed in the genetic models of blindness where the host photoreceptors are non-functional but still present [62].

We employed hES-derived RPE and primary mouse photoreceptors for transplantation. Clinical studies using pluripotent stem cell-derived RPE for AMD and Stargardt's macular dystrophy, currently underway in the United States, the United Kingdom and Japan, underline their clinical relevance [63]. Given the symbiotic relationship between RPE and photoreceptors and their degeneration in diseases like AMD and retinitis pigmentosa, vision repair in advanced stages of these diseases, as emulated herein, requires co-transplantation of both cell types.

We acknowledge that co-transplantation of murine photoreceptors and hES-derived RPE is a limitation of our study. Photoreceptors have been derived from human pluripotent stem cell populations [15,36–39], but their use is hindered by the current lack of knowledge on the optimal developmental stage for transplantation of these cells. Efforts to identify surface markers that will enable the purification of such integration-capable photoreceptors from human stem cell sources, as has previously been demonstrated for early postnatal mouse photoreceptors [64,65], are currently under investigation [66].

We observed statistically significant scotopic visual recovery only in co-transplanted animals using OKT, light avoidance and full field ERG. Co-transplanted animals recovered approximately 10.4% of their scotopic visual function by OKT, which is a quantitative assay that requires higher order vision to observe a bigger change [22,43]. Even though extrapolating such data to humans is difficult [67], small improvements in visual acuity can lead to significant changes in a patient's quality of life, enabling visually-guided behaviors such as object localization and obstacle avoidance [68].

Co-transplanted animals performed similarly to wild type controls in the light avoidance assay, which measures gross mouse behavior (time spent in compartments and activity therein) and may be more qualitative, requiring a lower threshold of visual perception to trigger the complete magnitude of the response. Similar tests, depending on rudimentary light perception, have demonstrated complete recovery of blind mice by therapeutic interventions in other settings [22,69]. Light aversion testing has been widely employed in assessing mouse anxiety levels [47]. To ensure that anxiety was not a contributing factor to the observed differences, we demonstrated that neither the number of entrances in the lit chamber nor the fecal boli produced were different among the groups.

Interestingly, behavioral recovery was observed in the scotopic light range, which is consistent with the physiological role of rods for night vision. This finding is compelling because it suggests that the behavioral recovery observed is mediated by rod photoreceptors. Host rods expressed visual cycle proteins and donor rods both expressed

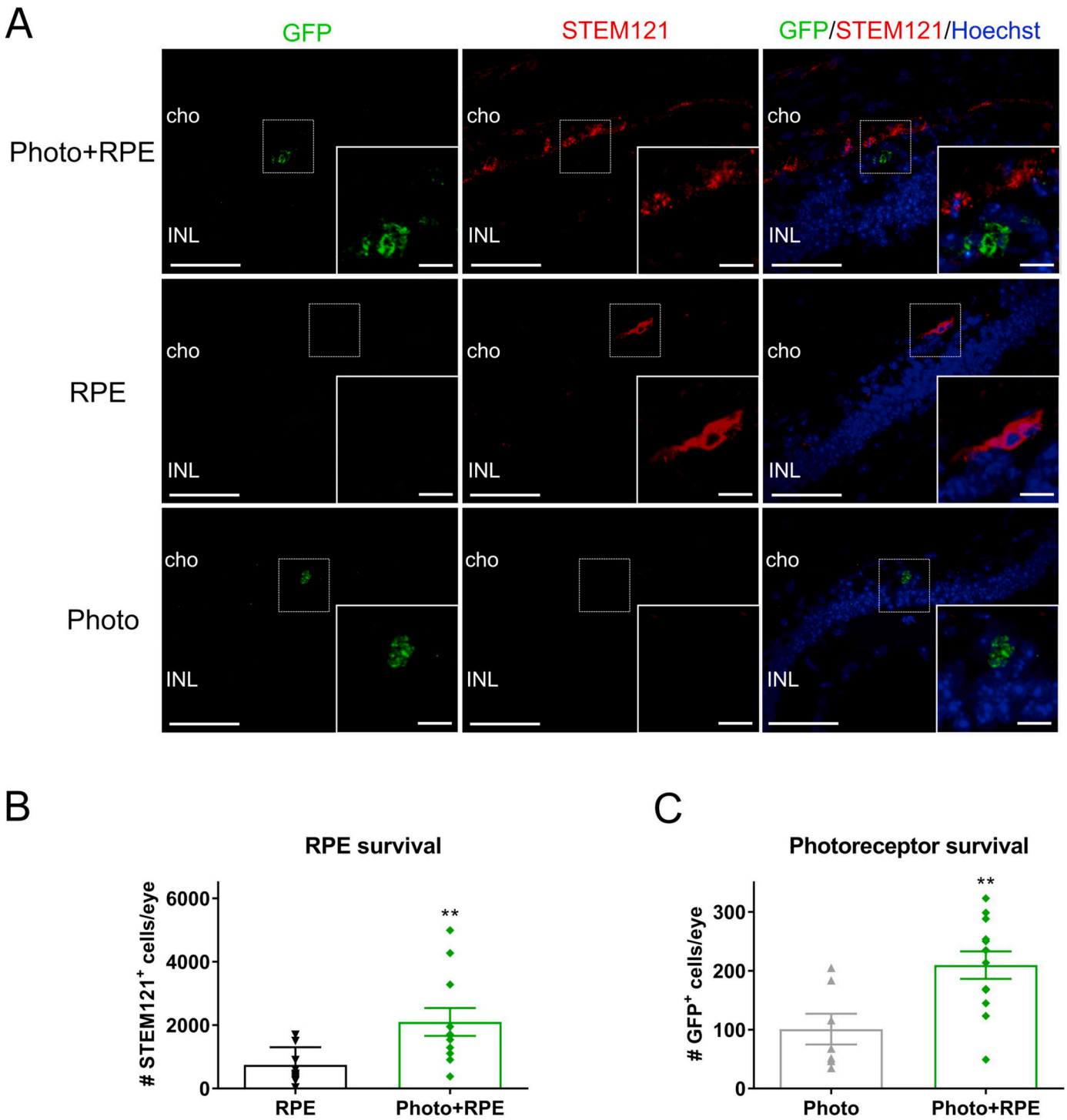


**Fig. 4.** Co-transplantation in HAMC leads to increased survival for both RPE and photoreceptors. (A) Representative immunohistochemistry images of donor photoreceptors and RPE in animals transplanted with both cell types, RPE alone, or photoreceptors alone, stained for GFP and human-specific STEM121. The dashed line boxes are magnified in the insets. Cho, choroid; INL, inner nuclear layer. Scale bars are 50 μm for the images and 10 μm for the insets. Secondary antibody control staining is shown in Supplementary Fig. 7C. (B) More donor RPE cells survive in co-transplanted animals compared to animals transplanted with RPE alone (mean ± SEM, n = 12 eyes for RPE, n = 11 eyes for Photo + RPE). Statistical comparison was performed by a 2-tailed, Mann Whitney test. **p < 0.01. (C) More donor photoreceptors survive in co-transplanted animals compared to animals transplanted with photoreceptors alone (mean ± SEM, n = 7 eyes for Photo, n = 12 eyes for Photo + RPE). Statistical comparison was performed by a 2-tailed, unpaired *t*-test. **p < 0.01.

synaptophysin and their numbers correlated with ERG signals. Since cone photoreceptors die before rods, and within weeks after $NaIO_3$ administration [70], the absence of both host and donor cones explains the absence of behavioral responses in photopic conditions.

Consistent with the well-established mutual relationship between RPE and photoreceptors, we found that cell survival was significantly greater for both cell types in the co-transplant group than when each cell type was transplanted alone. We attribute the lower overall donor photoreceptor survival compared to that reported by others [8,15,18,53] to: (1) our aggressive degeneration model; (2) our assessment of

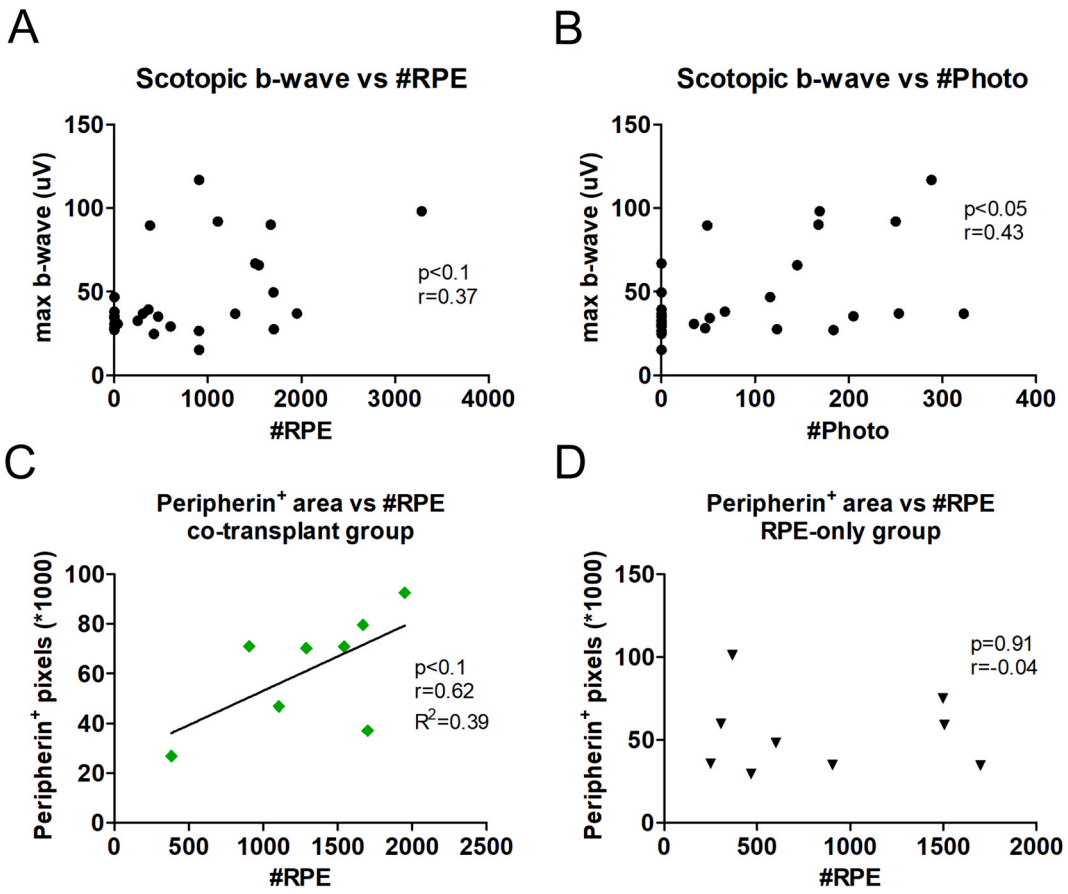


**Fig. 5.** The enhanced survival of each of RPE and photoreceptors when transplanted together correlates with ERG b-wave values. (A) Donor RPE numbers correlate with the maximum value in the ERG scotopic b-wave for individual eyes, pooled from groups transplanted with cells. n = 28 eyes, $p < 0.10$ ($p = 0.056$), Spearman r = 0.37. (B) Donor photoreceptor numbers correlate with the maximum value in the ERG scotopic b-wave for individual eyes, pooled from groups transplanted with cells. n = 27 eyes, $p < 0.05$, Spearman r = 0.43. (C) Peripherin$^+$ area correlates with donor RPE numbers in the co-transplant group. n = 8 eyes, $p < 0.10$ ($p = 0.099$), Pearson r = 0.62, $R^2 = 0.39$ for linear regression. (D) However, peripherin$^+$ area does not correlate with donor RPE numbers in the RPE alone group, reflecting the importance of co-transplantation for tissue repair. n = 9 eyes, p = 0.91, Pearson r = −0.04.

survival at 8 weeks post-transplantation as opposed to the typical 3–4 weeks, where there is greater survival [71]; and (3) the prevalence of GFP transfer with transplantation into structurally intact retinas (unlike those in this study), which leads to an overestimation of donor cell survival [11–13,62]. Importantly, there were statistically significant correlations between surviving numbers of both cell types and ERG. These correlations were of moderate strength, potentially reflecting that the mechanism of action of our transplants is complex, and involves donor-host interactions. While transplanted RPE should enable any surviving host photoreceptors to function, our data demonstrate that RPE transplantation alone is insufficient for behavioral recovery. The lack of visual recovery in the $NaIO_3$ mouse model after RPE-only transplants is consistent with other reports where both hES-derived and adult stem cell-derived RPE were transplanted without functional repair [34,72]. Even though we observed no evidence of host RPE proliferation after $NaIO_3$ administration, we acknowledge that the lack of donor RPE reporter labeling is a limitation of our study.

The combined delivery of photoreceptors and RPE is essential to scotopic visual recovery; however, the mechanism by which the transplanted rods contribute to behavioral amelioration remains unclear. The small number of surviving donor rods along with their immature morphology renders it unlikely that these cells alone are sufficient to produce useful vision. The donor photoreceptors may have promoted transplanted RPE survival, which in turn enhanced scotopic vision through surviving donor and host photoreceptors. This hypothesis is supported by the increased donor RPE numbers detected in the co-transplant group, compared to the RPE alone group, and the observed correlation of ERG signal with the number of surviving RPE. This suggests that there is a lower threshold of RPE survival, below which vision cannot be achieved. On the one hand, the co-transplantation of RPE with rods modulated the interaction of donor RPE with host photoreceptors as indicated by the correlation between donor RPE numbers and host peripherin staining, which was only observed in the co-transplant group. On the other hand, the donor rods may have secreted signals that potentiated the function of host rods. Such candidate factors include: the full-length isoform of rod-derived cone viability factor (RdCVFL) [73], which is produced by rods; and all-*trans* retinol, secreted by photoreceptors as a by-product of the visual cycle. Viral delivery of RdCVFL sustained rod function in the *rd10* mouse model of retinal degeneration without affecting cones [74]. All-*trans* retinol was recently demonstrated to augment the light sensitivity of rods through the insulin-like growth factor 1 pathway [75]. These hypotheses are not mutually exclusive; it is possible that the donor rods exerted trophic effects on both donor RPE and host rods. There is a paucity of knowledge in the literature regarding specific mechanisms of photoreceptor-induced RPE survival, and this would represent a compelling area for future research.

In conclusion, we developed a novel, minimally invasive approach to reverse blindness at an advanced stage of retinal degeneration. Delivering photoreceptors together with RPE in an injectable hyaluronan-methylcellulose hydrogel improved the outcome of cell transplantation at the tissue level and led to behavioral recovery. These results provide a pathway forward for future research and translation of

cell transplantation approaches for blindness.

## Author contributions

NM and MSS designed the experiments. NM, SH and MH performed the experiments. NM collected and analyzed the data. YS analyzed the ERG data. NM, DvdK, AN and MSS interpreted the data. NM and MSS wrote the manuscript.

## Data availability

All data will be available on Mendeley Data, in a dataset entitled "Original Data: Hydrogel-mediated co-transplantation of retinal pigmented epithelium and photoreceptors restores vision in an animal model of advanced retinal degeneration".

## Declaration of competing interest

The authors declare the following financial interests/personal relationships which may be considered as potential competing interests: The authors have no conflicts of interest to declare, but acknowledge a composition of matter patent on HAMC cell delivery.

## Acknowledgments

The authors would like to thank Katariina Mamia and Zhengyue (Leo) Zhu for their help with tissue processing, Peter Poon and Ricky Siu for their help with tail-vein injections, Beatrice Ballarin for her help with animal surgeries, Dr. Arturo Ortin-Martinez for his help with immunostaining, troubleshooting and flatmount preparations, Lacrimioara Comanita, Enleh Tsai and Dr. Valerie Wallace for their help with ERG, Dr. Alison McGuigan for providing ARPE19 cells, and members of the Shoichet lab for thoughtful review of this manuscript. Funding: NM is the recipient of an NSERC CREATE in M3 award and a University Health Network VSRP award. MSS, VAW, DvdK AN are grateful for partial funding from: the Canada First Research Excellence Fund for funding through Medicine by Design, the Ontario Institute for Regenerative Medicine, and the Krembil Foundation.

## Appendix A. Supplementary data

Supplementary data to this article can be found online at https://doi.org/10.1016/j.biomaterials.2020.120233.

## References

[1] O. Strauss, The retinal pigment epithelium in visual function, Physiol. Rev. 85 (2005) 845–881.
[2] J.G. Hollyfield, P. Witkovsky, Pigmented retinal epithelium involvement in photoreceptor development and function, J. Exp. Zool. 189 (1974) 357–378.
[3] A.R. Caffe, H. Visser, H.G. Jansen, S. Sanyal, Histotypic differentiation of neonatal mouse retina in organ culture, Curr. Eye Res. 8 (1989) 1083–1092.
[4] J.W. Miller, S. Bagheri, D.G. Vavvas, Advances in age-related macular degeneration understanding and therapy, US Ophthal. Rev. 10 (2017) 119–130.
[5] A.H. Milam, Z.Y. Li, R.N. Fariss, Histopathology of the human retina in retinitis pigmentosa, Prog. Retin. Eye Res. 17 (1998) 175–205.
[6] A. Santos, M.S. Humayun, E. de Juan Jr., R.J. Greenburg, M.J. Marsh, I.B. Klock, et al., Preservation of the inner retina in retinitis pigmentosa. A morphometric analysis, Arch. Ophthalmol. 115 (1997) 511–515.
[7] P.J. Coffey, S. Girman, S.M. Wang, L. Hetherington, D.J. Keegan, P. Adamson, et al., Long-term preservation of cortically dependent visual function in RCS rats by transplantation, Nat. Neurosci. 5 (2002) 53–56.
[8] R.E. MacLaren, R.A. Pearson, A. MacNeil, R.H. Douglas, T.E. Salt, M. Akimoto, et al., Retinal repair by transplantation of photoreceptor precursors, Nature 444 (2006) 203–207.
[9] M.S. Singh, P. Charbel Issa, R. Butler, C. Martin, D.M. Lipinski, S. Sekaran, et al., Reversal of end-stage retinal degeneration and restoration of visual function by photoreceptor transplantation, Proc. Natl. Acad. Sci. U. S. A. 110 (2013) 1101–1106.
[10] B. Lu, C. Malcuit, S. Wang, S. Girman, P. Francis, L. Lemieux, et al., Long-term safety and function of RPE from human embryonic stem cells in preclinical models of macular degeneration, Stem Cell. 27 (2009) 2126–2135.
[11] T. Santos-Ferreira, S. Llonch, O. Borsch, K. Postel, J. Haas, M. Ader, Retinal transplantation of photoreceptors results in donor-host cytoplasmic exchange, Nat. Commun. 7 (2016) 13028.
[12] M.S. Singh, J. Balmer, A.R. Barnard, S.A. Aslam, D. Moralli, C.M. Green, et al., Transplanted photoreceptor precursors transfer proteins to host photoreceptors by a mechanism of cytoplasmic fusion, Nat. Commun. 7 (2016) 13537.
[13] A. Ortin-Martinez, E.L. Tsai, P.E. Nickerson, M. Bergeret, Y. Lu, S. Smiley, et al., A reinterpretation of cell transplantation: GFP transfer fromdonor to host photoreceptors, Stem Cell. 35 (2017) 932–939.
[14] A.C. Barber, C. Hippert, Y. Duran, E.L. West, J.W. Bainbridge, K. Warre-Cornish, et al., Repair of the degenerate retina by photoreceptor transplantation, Proc. Natl. Acad. Sci. U. S. A. 110 (2013) 354–359.
[15] A.O. Barnea-Cramer, W. Wang, S.J. Lu, M.S. Singh, C. Luo, H. Huo, et al., Function of human pluripotent stem cell-derived photoreceptor progenitors in blind mice, Sci. Rep. 6 (2016) 29784.
[16] K. Kruczek, A. Gonzalez-Cordero, D. Goh, A. Naeem, M. Jonikas, S.J.I. Blackford, et al., Differentiation and transplantation of embryonic stem cell-derived cone photoreceptors into a mouse model of end-stage retinal degeneration, Stem Cell Rep. 8 (2017) 1659–1674.
[17] S.D. Schwartz, C.D. Regillo, B.L. Lam, D. Eliott, P.J. Rosenfeld, N.Z. Gregori, et al., Human embryonic stem cell-derived retinal pigment epithelium in patients with age-related macular degeneration and Stargardt's macular dystrophy: follow-up of two open-label phase 1/2 studies, Lancet 385 (2015) 509–516.
[18] R.A. Pearson, A.C. Barber, M. Rizzi, C. Hippert, T. Xue, E.L. West, et al., Restoration of vision after transplantation of photoreceptors, Nature 485 (2012) 99–103.
[19] L. da Cruz, K. Fynes, O. Georgiadis, J. Kerby, Y.H. Luo, A. Ahmado, et al., Phase 1 clinical study of an embryonic stem cell-derived retinal pigment epithelium patch in age-related macular degeneration, Nat. Biotechnol. 36 (2018) 328–337.
[20] A.H. Kashani, J.S. Lebkowski, F.M. Rahhal, R.L. Avery, H. Salehi-Had, W. Dang, et al., A bioengineered retinal pigment epithelial monolayer for advanced, dry age-related macular degeneration, Sci. Transl. Med. 10 (2018), https://doi.org/10.1126/scitranslmed.aao4097.
[21] K. Ben M'Barek, W. Habeler, A. Plancheron, M. Jarraya, F. Regent, A. Terray, et al., Human ESC-derived retinal epithelial cell sheets potentiate rescue of photoreceptor cell loss in rats with retinal degeneration, Sci. Transl. Med. 9 (2017), https://doi.org/10.1126/scitranslmed.aai7471.
[22] M. Mandai, M. Fujii, T. Hashiguchi, G.A. Sunagawa, S.I. Ito, J. Sun, et al., iPSC-derived retina transplants improve vision in rd1 end-stage retinal-degeneration mice, Stem Cell Rep. 8 (2017) 1112–1113.
[23] E.B. Lavik, H. Klassen, K. Warfvinge, R. Langer, M.J. Young, Fabrication of degradable polymer scaffolds to direct the integration and differentiation of retinal progenitors, Biomaterials 26 (2005) 3187–3196.
[24] H. Kamao, M. Mandai, W. Ohashi, Y. Hirami, Y. Kurimoto, J. Kiryu, et al., Evaluation of the surgical device and procedure for extracellular matrix-scaffold-supported human iPSC-derived retinal pigment epithelium cell sheet transplantation, Invest. Ophthalmol. Vis. Sci. 58 (2017) 211–220.
[25] Y. Hu, L. Liu, B. Lu, D. Zhu, R. Ribeiro, B. Diniz, et al., A novel approach for subretinal implantation of ultrathin substrates containing stem cell-derived retinal pigment epithelium monolayer, Ophthalmic Res. 48 (2012) 186–191.
[26] B. Diniz, P. Thomas, B. Thomas, R. Ribeiro, Y. Hu, R. Brant, et al., Subretinal implantation of retinal pigment epithelial cells derived from human embryonic stem cells: improved survival when implanted as a monolayer, Invest. Ophthalmol. Vis. Sci. 54 (2013) 5087–5096.
[27] E.J. van Zeeburg, K.J. Maaijwee, T.O. Missotten, H. Heimann, J.C. van Meurs, A free retinal pigment epithelium-choroid graft in patients with exudative age-related macular degeneration: results up to 7 years, Am. J. Ophthalmol. 153 (2012) 120–127, e2.
[28] B.A. Aguado, W. Mulyasasmita, J. Su, K.J. Lampe, S.C. Heilshorn, Improving viability of stem cells during syringe needle flow through the design of hydrogel cell carriers, Tissue Eng. Part A 18 (2012) 806–815.
[29] N. Mitrousis, A. Fokina, M.S. Shoichet, Biomaterials for cell transplantation, Nat. Rev. Mater. (2018).
[30] B.G. Ballios, M.J. Cooke, L. Donaldson, B.L. Coles, C.M. Morshead, D. van der Kooy, et al., A hyaluronan-based injectable hydrogel improves the survival and integration of stem cell progeny following transplantation, Stem Cell Rep. 4 (2015) 1031–1045.
[31] N. Mitrousis, R.Y. Tam, A.E.G. Baker, D. van der Kooy, M.S. Shoichet, Hyaluronic acid-based hydrogels enable rod photoreceptor survival and maturation invitro through activation of the mTOR pathway, Adv. Funct. Mater. 26 (2016) 1975–1985.
[32] D. Gupta, C.H. Tator, M.S. Shoichet, Fast-gelling injectable blend of hyaluronan and methylcellulose for intrathecal, localized delivery to the injured spinal cord, Biomaterials 27 (2006) 2370–2379.
[33] A. Sorsby, Experimental pigmentary degeneration of the retina by sodium iodate, Br. J. Ophthalmol. 25 (1941) 58–62.
[34] M. Carido, Y. Zhu, K. Postel, B. Benkner, P. Cimalla, M.O. Karl, et al., Characterization of a mouse model with complete RPE loss and its use for RPE cell transplantation, Invest. Ophthalmol. Vis. Sci. 55 (2014) 5431–5444.
[35] S.Y. Kim, S. Sadda, M.S. Humayun, E. de Juan Jr., B.M. Melia, W.R. Green, Morphometric analysis of the macula in eyes with geographic atrophy due to age-related macular degeneration, Retina 22 (2002) 464–470.
[36] H. Shirai, M. Mandai, K. Matsushita, A. Kuwahara, S. Yonemura, T. Nakano, et al., Transplantation of human embryonic stem cell-derived retinal tissue in two primate models of retinal degeneration, Proc. Natl. Acad. Sci. U. S. A. 113 (2016) E81–E90.

[37] S. Zhou, A. Flamier, M. Abdouh, N. Tetreault, A. Barabino, S. Wadhwa, et al., Differentiation of human embryonic stem cells into cone photoreceptors through simultaneous inhibition of BMP, TGFbeta and Wnt signaling, Development 142 (2015) 3294–3306.
[38] J. Zhu, J. Reynolds, T. Garcia, H. Cifuentes, S. Chew, X. Zeng, et al., Generation of transplantable retinal photoreceptors from a current good manufacturing practice-manufactured human induced pluripotent stem cell line, Stem Cells Transl. Med. 7 (2018) 210–219.
[39] J. Collin, D. Zerti, R. Queen, T. Santos-Ferreira, R. Bauer, J. Coxhead, et al., CRX expression in pluripotent stem cell-derived photoreceptors marks a transplantable subpopulation of early cones, Stem Cell. 37 (2019) 609–622.
[40] J. Gust, T.A. Reh, Adult donor rod photoreceptors integrate into the mature mouse retina, Invest. Ophthalmol. Vis. Sci. 52 (2011) 5266–5272.
[41] M. Akimoto, H. Cheng, D. Zhu, J.A. Brzezinski, R. Khanna, E. Filippova, et al., Targeting of GFP to newborn rods by Nrl promoter and temporal expression profiling of flow-sorted photoreceptors, Proc. Natl. Acad. Sci. U. S. A. 103 (2006) 3890–3895.
[42] J. Parker, N. Mitrousis, M.S. Shoichet, Hydrogel for simultaneous tunable growth factor delivery and enhanced viability of encapsulated cells in vitro, Biomacromolecules 17 (2016) 476–484.
[43] G.T. Prusky, N.M. Alam, S. Beekman, R.M. Douglas, Rapid quantification of adult and developing mouse spatial vision using a virtual optomotor system, Invest. Ophthalmol. Vis. Sci. 45 (2004) 4611–4616.
[44] N.M. Alam, C.M. Altimus, R.M. Douglas, S. Hattar, G.T. Prusky, Photoreceptor regulation of spatial visual behavior, Invest. Ophthalmol. Vis. Sci. 56 (2015) 1842–1849.
[45] J. Schindelin, I. Arganda-Carreras, E. Frise, V. Kaynig, M. Longair, T. Pietzsch, et al., Fiji: an open-source platform for biological-image analysis, Nat. Methods 9 (2012) 676–682.
[46] A. Tuladhar, C.M. Morshead, M.S. Shoichet, Circumventing the blood-brain barrier: local delivery of cyclosporin A stimulates stem cells in stroke-injured rat brain, J. Control Release 215 (2015) 1–11.
[47] M. Bourin, M. Hascoet, The mouse light/dark box test, Eur. J. Pharmacol. 463 (2003) 55–65.
[48] I. Klimanskaya, J. Hipp, K.A. Rezai, M. West, A. Atala, R. Lanza, Derivation and comparative assessment of retinal pigment epithelium from human embryonic stem cells using transcriptomics, Clon Stem Cell 6 (2004) 217–245.
[49] S. McLenachan, E. Hao, D. Zhang, L. Zhang, M. Edel, F. Chen, Bioengineered Bruch's-like extracellular matrix promotes retinal pigment epithelial differentiation, Biochem. Biophys. Rep. 10 (2017) 178–185.
[50] W. Samuel, C. Jaworski, O.A. Postnikova, R.K. Kutty, T. Duncan, L.X. Tan, et al., Appropriately differentiated ARPE-19 cells regain phenotype and gene expression profiles similar to those of native RPE cells, Mol. Vis. 23 (2017) 60–89.
[51] S. Thompson, R.G. Foster, E.M. Stone, V.C. Sheffield, N. Mrosovsky, Classical and melanopsin photoreception in irradiance detection: negative masking of locomotor activity by light, Eur. J. Neurosci. 27 (2008) 1973–1979.
[52] M.L. Seibenhener, M.C. Wooten, Use of the Open Field Maze to measure locomotor and anxiety-like behavior in mice, J. Vis. Exp. 96 (2015), e52434 e52434.
[53] D.A. Lamba, J. Gust, T.A. Reh, Transplantation of human embryonic stem cell-derived photoreceptors restores some visual function in Crx-deficient mice, Cell Stem Cell 4 (2009) 73–79.
[54] G.H. Travis, M. Golczak, A.R. Moise, K. Palczewski, Diseases caused by defects in the visual cycle: retinoids as potential therapeutic agents, Annu. Rev. Pharmacol. Toxicol. 47 (2007) 469–512.
[55] M.J. Seiler, R.E. Lin, B.T. McLelland, A. Mathur, B. Lin, J. Sigman, et al., Vision recovery and connectivity by fetal retinal sheet transplantation in an immunodeficient retinal degenerate rat model, Invest. Ophthalmol. Vis. Sci. 58 (2017) 614–630.
[56] B. Juliusson, A. Bergstrom, T. van Veen, B. Ehinger, Cellular organization in retinal transplants using cell suspensions or fragments of embryonic retinal tissue, Cell Transplant. 2 (1993) 411–418.
[57] R. Kannan, D.R. Hinton, Sodium iodate induced retinal degeneration: new insights from an old model, Neural Regen. Res. 9 (2014) 2044–2045.
[58] L.M. Franco, R. Zulliger, U.E. Wolf-Schnurrbusch, Y. Katagiri, H.J. Kaplan, S. Wolf, et al., Decreased visual function after patchy loss of retinal pigment epithelium induced by low-dose sodium iodate, Invest. Ophthalmol. Vis. Sci. 50 (2009) 4004–4010.
[59] G. Chowers, M. Cohen, D. Marks-Ohana, S. Stika, A. Eijzenberg, E. Banin, et al., Course of sodium iodate-induced retinal degeneration in Albino and pigmented mice, Invest. Ophthalmol. Vis. Sci. 58 (2017) 2239–2249.
[60] W. Wang, L.M. Franco, J.N. Brodfuehrer, M.L. Hamilton, M.M. McCall, D.C. Dean, et al., Evaluation of vision loss in mice following sodium iodate-induced retinal pigment epithelium (RPE) damage and RPE transplantation, IOVS (Investig. Ophthalmol. Vis. Sci.) 2162 (2009) 50.
[61] K. Kiuchi, K. Yoshizawa, N. Shikata, K. Moriguchi, A. Tsubura, Morphologic characteristics of retinal degeneration induced by sodium iodate in mice, Curr. Eye Res. 25 (2002) 373–379.
[62] P.V. Waldron, F. Di Marco, K. Kruczek, J. Ribeiro, A.B. Graca, C. Hippert, et al., Transplanted donor- or stem cell-derived cone photoreceptors can both integrate and undergo material transfer in an environment-dependent manner, Stem Cell Reports 10 (2018) 406–421.
[63] M. Fields, H. Cai, J. Gong, L. Del Priore, Potential of induced pluripotent stem cells (iPSCs) for treating age-related macular degeneration (AMD), Cells 5 (2016), https://doi.org/10.3390/cells5040044.
[64] D. Eberle, S. Schubert, K. Postel, D. Corbeil, M. Ader, Increased integration of transplanted CD73-positive photoreceptor precursors into adult mouse retina, Invest. Ophthalmol. Vis. Sci. 52 (2011) 6462–6471.
[65] J. Lakowski, Y.T. Han, R.A. Pearson, A. Gonzalez-Cordero, E.L. West, S. Gualdoni, et al., Effective transplantation of photoreceptor precursor cells selected via cell surface antigen expression, Stem Cell. 29 (2011) 1391–1404.
[66] J. Lakowski, E. Welby, D. Budinger, F. Di Marco, V. Di Foggia, J.W.B. Bainbridge, et al., Isolation of human photoreceptor precursors via a cell surface marker panel from stem cell-derived retinal organoids and fetal retinae, Stem Cell. (2018).
[67] D. Birch, F. Fitzke, G. Rubin, Chapter 8-restoring vision to the blind: evaluating visual function, endpoints, Transl. Vis. Sci. Technol. 3 (2014) 10.
[68] E. Zrenner, B. Greger, Chapter 1-restoring vision to the blind: the new age of implanted visual prostheses, Transl. Vis. Sci. Technol. 3 (2014) 3.
[69] I. Tochitsky, A. Polosukhina, V.E. Degtyar, N. Gallerani, C.M. Smith, A. Friedman, et al., Restoring visual function to blind mice with a photoswitch that exploits electrophysiological remodeling of retinal ganglion cells, Neuron 81 (2014) 800–813.
[70] W. Wang, J. Noel, H.J. Kaplan, D.C. Dean, Circulating reactive oxidant causes apoptosis of retinal pigment epithelium and cone photoreceptors in the mouse central retina, Ophthalmol. Eye Dis. 3 (2011) 45–54.
[71] E.L. West, R.A. Pearson, S.E. Barker, U.F. Luhmann, R.E. Maclaren, A.C. Barber, et al., Long-term survival of photoreceptors transplanted into the adult murine neural retina requires immune modulation, Stem Cell. 28 (2010) 1997–2007.
[72] S. Lecaudé, U.E.K. Wolf-schnurrbusch, H. Abdullahi, V. Enzmann, Bone marrow-derived stem cells differentiate into retinal pigment epithelium-like cells in vitro but are not able to repair retinal degeneration in vivo, Stem Cell Transl. Invest. 2 (2015), 1–2-10.
[73] X. Mei, A. Chaffiol, C. Kole, Y. Yang, G. Millet-Puel, E. Clerin, et al., The thioredoxin encoded by the rod-derived cone viability factor gene protects cone photoreceptors against oxidative stress, Antioxid. Redox Signal 24 (2016) 909–923.
[74] L.C. Byrne, D. Dalkara, G. Luna, S.K. Fisher, E. Clerin, J.A. Sahel, et al., Viral-mediated RdCVF and RdCVFL expression protects cone and rod photoreceptors in retinal degeneration, J. Clin. Invest. 125 (2015) 105–116.
[75] A.S. McKeown, P.M. Pitale, T.W. Kraft, Signalling beyond photon absorption: extracellular retinoids and growth factors modulate rod photoreceptor sensitivity, J. Physiol. 594 (2016) 1841–1854.